K06

Proceedings of the 5th International Conference on Inverse Problems in Engineering: Theory and Practice, Cambridge, UK, 11-15th July 2005

NONSTATIONARY BOUNDARY ESTIMATION IN ELECTRICAL IMPEDANCE TOMOGRAPHY BASED ON THE IMM SCHEME

B.S. Kim[1], U.Z. Ijaz[1], J.H. Kim[1], M.C. Kim[2], S. Kim[3] and K.Y Kim[1]
[1] *Department of Electrical and Electronic Engineering, Cheju National University, Cheju 690-756, Korea*
e-mail: kyungyk@cheju.ac.kr
[2] *Department of Chemical Engineering, Cheju National University, Cheju 690-756, Korea*
[3] *Department of Nuclear and Energy Engineering, Cheju National University, Cheju 690-756, Korea*

Abstract - In this paper, an effective nonstationary boundary estimation scheme in EIT is presented based on the interacting multiple model (IMM) algorithm. The inverse problem is treated as a stochastic nonlinear state estimation problem with the time-varying boundary (state) being estimated on-line with the aid of the IMM algorithm. In the design of the IMM algorithm multiple models with different process noise covariances are incorporated to reduce the modeling uncertainty. Simulations are provided to illustrate the proposed algorithm.

1. INTRODUCTION

Image reconstruction in electrical impedance tomography (EIT) is a kind of nonlinear optimization problem in which the solution is obtained iteratively through the forward and inverse solvers. The physical relationship between the internal resistivity and the surface voltage is governed by a partial differential equation (Laplace equation) with appropriate boundary conditions. It is in most cases impossible to obtain an analytical solution for the forward problem so that the numerical technique such as the finite element method (FEM) is often employed. The inverse problem in EIT is a highly nonlinear and ill-posed problem. Hence, various reconstruction algorithms (inverse solvers) with different regularization methods have been developed in the literature [3, 6, 16] to estimate the internal resistivity distribution of the body.

Reconstruction algorithms presented so far have focused mainly on the case where the internal resistivity of the body is time-invariant within the time taken to acquire a full set of measurement data [19]. Therefore, these static imaging techniques often fail to obtain the satisfactory temporal resolution for the reconstructed images when a rapid change in the resistivity happens within data acquisition time.

In order to enhance the temporal resolution, so called 'dynamical imaging techniques' have been introduced for situations where the resistivity distribution inside the body changes rapidly. In these dynamical approaches, the temporal resolution can be improved by a factor of p times (p is the number of current patterns in 1 classical frame) at the expense of the spatial resolution. This result is due to the fact that the dynamical imaging technique provides an estimate for resistivity distribution after each current pattern is applied to the body. In most of these techniques, the inverse problem is treated as a nonlinear state estimation problem in which the time-varying state is estimated with the aid of a linearized Kalman filter (LKF) [16, 17] or extended Kalman filter (EKF) [9]. The state evolution model used in these dynamical approaches is the so-called random walk model in which the rate of evolution is governed by the covariance of the process noise. However, the modeling uncertainty of the random walk model may be large enough to cause significant negative effects on the quality of the reconstructed image.

To reduce the modeling uncertainty and improve the spatial resolution, dynamical imaging techniques in which a fluid dynamical evolution model was formulated, have been applied successfully to process tomography [14]. In these approaches, the state transition matrix is obtained from the known dynamics of fluids. In addition, multiple kinematic models have been incorporated into the interacting multiple model (IMM) algorithm [1, 13] to estimate the nonstationary resistivity distribution [7, 8].

In the present study we address a special class of the EIT inverse problem, in which position and shape of the objects in the domain are the unknowns to be identified [5, 10, 11]. In particular, it is assumed that these unknowns are nonstationary within the time taken to acquire a full set of measurement data. Considered situations of the type may arise for example in two-phase flow, in which the air bubbles can appear and disappear abruptly. In the medical applications, the boundaries of lungs and heart in the chest may vary with time according to the respirational and cardiac cycle, respectively. The state estimation approach to identify nonstationary position and shape of the objects has been introduced by Vauhkonen *et al.* [17], in which phase boundary is expressed as truncated Fourier series and the Fourier coefficients are estimated dynamically with the aid of the both LKF and Kalman smoother. Recently, the EKF has been applied to the estimation of nonstationary region boundary [12].

In this paper, an effective nonstationary boundary estimation scheme in EIT is presented based on the interacting multiple model (IMM) algorithm. The EIT boundary estimation problem is treated as a stochastic nonlinear state estimation problem. Multiple state evolution models with different process noise covariances are incorporated into the IMM algorithm. The generalized Tikhonov regularization scheme is incorporated into the cost functional to mitigate the ill-conditioned characteristics. The proposed IMM-based boundary estimation scheme is a recursive estimator and consists of a bank of model-conditioned extended Kalman filters connected in parallel, a model probability evaluator, an estimate mixer at the input of each Kalman filter, and an estimate combiner at the output of the parallel filters.

Extensive computer simulations are provided to illustrate the enhanced estimation performance.

2. MATHEMATICAL MODELING AND FORWARD SOLVER

When electrical currents I_l $(l = 1, 2, \ldots, L)$ are injected into a body $\Omega \in \mathbb{R}^2$ through the electrodes e_l $(l = 1, 2, \ldots, L)$ attached on the boundary $\partial\Omega$, and the resistivity distribution $\rho(x, y)$ is known for Ω, the corresponding electrical potential $u(x, y)$ on Ω can be determined uniquely from a partial differential equation, which can be derived from the Maxwell equations:

$$\nabla \cdot (\rho^{-1} \nabla u) = 0 \quad \text{in } \Omega \tag{1}$$

with the following boundary conditions based on the complete electrode model:

$$u + z_l \rho^{-1} \frac{\partial u}{\partial n} = \bar{u}_l \quad \text{on } e_l,\ l = 1, 2, \ldots, L \tag{2a}$$

$$\int_{e_l} \rho^{-1} \frac{\partial u}{\partial n} \, \mathrm{d}S = I_l, \quad l = 1, 2, \ldots, L \tag{2b}$$

$$\rho^{-1} \frac{\partial u}{\partial n} = 0 \quad \text{on } \partial\Omega \backslash \bigcup_{l=1}^{L} e_l \tag{2c}$$

where, z_l is the effective contact impedance between the l-th electrode and electrolyte, $\bar{u}_l$ is the potential on the l-th electrode, e_l is the l-th electrode, n is the outward unit normal, and L is the number of the electrodes. Various forms of boundary conditions may be used in the forward model [18]. We have chosen the complete electrode model (CEM) [15, 16], which takes into account the discrete electrodes, effects of the contact impedance, and the shunting effect of the electrodes. In addition, the following two constraints for the injected currents and measured voltages ensure the existence and uniqueness of the solution:

$$\sum_{l=1}^{L} I_l = 0, \sum_{l=1}^{L} \bar{u}_l = 0. \tag{3}$$

The computation of the potential $u(x, y)$ on Ω and the voltages $\bar{u}_l$ on the electrodes for the given resistivity distribution $\rho(x, y)$ and boundary conditions is called the forward problem. In general, the forward problem can not be solved analytically, so we have to resort to a numerical method. There are different numerical methods such as the finite difference method (FDM), boundary element method (BEM), and finite element method (FEM). In this paper, we used the FEM to obtain a numerical solution. In the FEM, the object area is discretized into sufficiently small elements having a node at each corner, while it is assumed that the resistivity distribution is constant within each element. The potential at each node, and the "referenced" electrode voltages, defined by the vector $v \in \mathbb{R}^{N_n+L-1}$, are calculated by discretizing (1) into $Yv = c$, where $Y \in \mathbb{R}^{(N_n+L-1)\times(N_n+L-1)}$ is the so-called stiffness matrix and N_n is the number of FEM nodes. Y and c are functions of the resistivity distribution in the object and the injected currents through the electrodes, respectively. For more details on the forward solution and the FEM approach, see [16].

3. INVERSE SOLVER WITH IMM ALGORITHM

3.1. Expression of phase boundaries

We assume that the outer boundary of the body, that is, $\partial\Omega$ is known. If the boundaries of the objects are sufficiently smooth, they can be approximated in the form [11, 12]

$$C_l(s) = \begin{pmatrix} x_l(s) \\ y_l(s) \end{pmatrix} = \sum_{n=1}^{N_\theta} \begin{pmatrix} \gamma_n^{x_l} \theta_n^x(s) \\ \gamma_n^{y_l} \theta_n^y(s) \end{pmatrix} \tag{4}$$

where $C_l(s)$, $(l = 1, 2, \ldots, S)$ is the boundary of the l-th object, S is the number of the objects in the body, $\theta_n(s)$ are periodic and differentiable basis functions, and N_θ is the number of basis functions. In this paper we express both coordinates of the curve as Fourier series with respect to the parameter s, that is, we use basis functions of the form

$$\begin{aligned} \theta_1^\alpha(s) &= 1 \\ \theta_n^x(s) &= \sin(2n\pi s), \quad n = 2, 3, \ldots \\ \theta_n^y(s) &= \cos(2n\pi s), \quad n = 2, 3, \ldots \end{aligned} \tag{5}$$

where $s \in [0, 1]$ and α denotes either x or y. Furthermore, using the expansion (4), the boundaries are identified with the vector γ of the shape coefficients, that is,

$$\gamma = \left(\gamma_1^{x_1}, \ldots, \gamma_{N_\theta}^{x_1}, \gamma_1^{y_1}, \ldots, \gamma_{N_\theta}^{y_1}, \ldots, \ldots, \gamma_1^{x_S}, \ldots, \gamma_{N_\theta}^{x_S}, \gamma_1^{y_S}, \ldots, \gamma_{N_\theta}^{y_S}\right)^{tr} \tag{6}$$

where $\gamma \in \mathbb{R}^{2SN_\theta}$.

3.2. Dynamic model and inverse solver

3.2.1. Formulation of dynamic model. We consider the underlying inverse problem as a state estimation problem to estimate the time-varying boundaries in the domain. We assume that the resistivity values of the objects are known constants. We also assume that the problem has been discretized with respect to the time variable. In the state estimation problem, we need the so-called dynamic model which consists of the state equation, that is, the evolution of the boundaries, and the observation equation, that is, the relationship between the boundary vector and measured voltages.

First, consider the state evolution model. In general, the evolution of the boundary vector γ is related by the following nonlinear mapping;

$$\gamma_{k+1} = g_k(\gamma_k) + w_k \tag{7}$$

where γ_k is the state vector (the boundary representation) at time kT, g_k is a function ($g_k : \mathbb{R}^{2SN_\theta} \longmapsto \mathbb{R}^{2SN_\theta}$) defineing the state transition from time kT to $(k + 1)T$, where T is the sampling period (measurement interval between successive patterns), and w_k is assumed to be white Gaussian noise to compensate for modeling uncertainty. Here, the state equation is assumed to be of linear form with different process noise:

$$\gamma_{k+1}^i = F_k\, \gamma_k^i + w_k^i \tag{8}$$

where $F_k \in \mathbb{R}^{2SN_\theta \times 2SN_\theta}$ is the state transition matrix at time kT, and $i = 1, 2, \ldots, M$, where M is the number of different models. Usually in EIT there is no *a priori* information on the time evolution of the boundary vector so that we take $F_k \equiv I$ (the identity matrix). Then (8) becomes the so-called random-walk model in which the rate of time evolution is governed by the different covariance matrices, defined by

$$Q_k^i = E[w_k^i\, (w_k^i)^T]. \tag{9}$$

Next, consider the observation model. Let $\bar{u}_k \in \mathbb{R}^L$, be defined as

$$\bar{u}_k \equiv [\bar{u}_k^1, \bar{u}_k^2, \ldots, \bar{u}_k^L]^{tr} \tag{10}$$

be the actual surface measurement voltages induced by the k-th current pattern. Then the relationship between the boundary vector and measured voltages can be described by the following nonlinear mapping with a measurement error

$$\bar{u}_k = h_k(\gamma_k) + \nu_k \tag{11}$$

where h_k is a function ($h_k; \mathbb{R}^{2SN_\theta} \longmapsto \mathbb{R}^L$) defining the relationship between the boundary vector and measured voltages for the k-th current pattern. The measurement error $\nu_k \in \mathbb{R}^L$ is assumed to be white Gaussian noise with covariance

$$R_k = E[\nu_k\, \nu_k^T]. \tag{12}$$

Linearizing (11) about the predicted (time-updated) states of i-th model $\gamma_{k|k-1}^i$, which will be described later in Subsection 3.2.2, we obtain

$$\bar{u}_k = h_k(\gamma_{k|k-1}^i) + J_k^i(\gamma_{k|k-1}^i) \cdot (\gamma_k^i - \gamma_{k|k-1}^i) + H.O.Ts + \nu_k \tag{13}$$

where $H.O.Ts$ represents the higher-order terms which are assumed to be additional white Gaussian noise, and $J_k^i(\gamma_{k|k-1}^i) \in \mathbb{R}^{L\times 2SN_\theta}$ is the Jacobian matrix defined by

$$J_k^i(\gamma_{k|k-1}^i) \equiv \left.\frac{\partial h_k}{\partial \gamma}\right|_{\gamma=\gamma_{k|k-1}^i}. \tag{14}$$

Let's define a pseudo-measurement as

$$y_k^i \equiv \bar{u}_k - h_k(\gamma_{k|k-1}^i) + J_k^i(\gamma_{k|k-1}^i)\cdot\gamma_{k|k-1}^i. \tag{15}$$

Then we can obtain the following linearized measurement equation:

$$y_k^i = J_k^i(\gamma_{k|k-1}^i)\cdot\gamma_k^i + \bar{\nu}_k \tag{16}$$

where $\bar{\nu}_k \in \mathbb{R}^L$ is composed of the measurement error and linearization error with known covariance as

$$\bar{R}_k = E[\bar{\nu}_k\,\bar{\nu}_k^{tr}]. \tag{17}$$

3.2.2. Extended Kalman filter. In Kalman filtering we estimate the state vector γ_k^i for each model based on all the measurements taken up to the time kT. With the Gaussian assumptions the required estimate is obtained by minimizing the cost functional which is formulated based on the above state and measurement equations (8) and (16), respectively. The cost functional for the extended Kalman filter (EKF) is of the form

$$\Xi^i(\gamma_k^i) = \frac{1}{2}\left[\|\gamma_k^i - \gamma_{k|k-1}^i\|_{(C_{k|k-1}^i)^{-1}} + \|y_k^i - J_k^i(\gamma_{k|k-1}^i)\cdot\gamma_k^i\|_{\bar{R}_k^{-1}} + \alpha\|R(\gamma_k^i - \gamma^*)\|\right] \tag{18}$$

where $\|x\|_A$ denotes $x^{tr}Ax$, α and $R \in \mathbb{R}^{2SN_\theta\times 2SN_\theta}$ are the regularization parameter and matrix, respectively, γ^* is an *a priori* guess for the boundary representation, and $C_{k|k-1}^i \in \mathbb{R}^{2SN_\theta\times 2SN_\theta}$ is the time-updated error covariance matrix, which is defined by

$$C_{k|k-1}^i \equiv E[(\gamma_k^i - \gamma_{k|k-1}^i)(\gamma_k^i - \gamma_{k|k-1}^i)^T]. \tag{19}$$

The first two norms in (18) refer to the weighted norms, having as weighting matrices the inverse of the covariances. The third term on the right-hand side of (18) is the regularization term which is included to mitigate the ill-posedness of the given inverse problem. We used the generalized Tikhonov regularization under a smoothness assumption in constructing the regularization matrix (R), with the regularization parameter α chosen empirically.

If we define the augmented pseudo-measurement $\bar{y}_k^i \in \mathbb{R}^{(L+2SN_\theta)}$ and measurement matrix $H_k^i \in \mathbb{R}^{(L+2SN_\theta)\times 2SN_\theta}$

$$\bar{y}_k^i \equiv \begin{pmatrix} y_k^i \\ \sqrt{\alpha}R\gamma^* \end{pmatrix} \tag{20}$$

$$H_k^i \equiv \begin{pmatrix} J_k^i(\gamma_{k|k-1}^i) \\ \sqrt{\alpha}R \end{pmatrix} \tag{21}$$

then the cost functional (18) can be rearranged as

$$\Xi^i(\gamma_k^i) = \frac{1}{2}\left[\|\gamma_k^i - \gamma_{k|k-1}^i\|_{(C_{k|k-1}^i)^{-1}} + \|\bar{y}_k^i - H_k^i\cdot\gamma_k^i\|_{\Gamma_k^{-1}}\right] \tag{22}$$

where $\Gamma_k \in \mathbb{R}^{(L+2SN_\theta)\times(L+2SN_\theta)}$ is a block diagonal matrix defined by

$$\Gamma_k \equiv \text{Blockdiag}[\bar{R}_k, I_{2SN_\theta}]. \tag{23}$$

Minimizing the cost functional (22) and solving for the updates of the associated covariance matrices, we obtain the recursive extended Kalman filter algorithm for each model, which consists of the following two steps [4]:

- time update (prediction)

$$\gamma_{k+1|k}^i = F_k\,\gamma_{k|k}^i \tag{24}$$

$$C_{k+1|k}^i = F_k\,C_{k|k}^i\,(F_k)^T + Q_k^i \tag{25}$$

- measurement update (filtering)

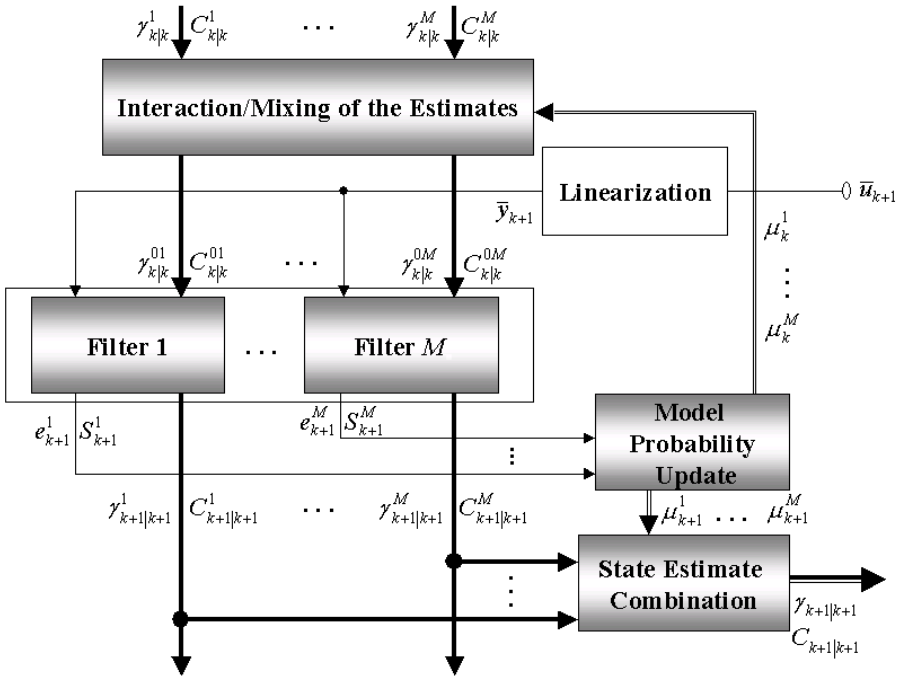

Figure 1. One-cycle flow diagram of the inverse solver with the IMM algorithm.

$$G^i_{k+1} = C^i_{k+1|k}\,(H^i_{k+1})^T\,[H^i_{k+1}\,C^i_{k+1|k}\,(H^i_{k+1})^T + \Gamma_{k+1}]^{-1} \tag{26}$$

$$\gamma^i_{k+1|k+1} = \gamma^i_{k+1|k} + G^i_{k+1}\,(\bar{y}^i_{k+1} - H^i_{k+1}\,\gamma^i_{k+1|k}) \tag{27}$$

$$C^i_{k+1|k+1} = (I_{2SN_\theta} - G^i_{k+1}\,H^i_{k+1})\,C^i_{k+1|k}. \tag{28}$$

Hence, we can find the estimated state $\gamma^i_{k|k}$ for model i for $k = 0, 1, 2, \ldots, K, (K = rp)$, where K is final step for the iteration, p is the number of the independent current patterns, and r is the number of the classical frames. The most striking feature is that the Kalman filtering technique is an on-line recursive form in place of the off-line batch form of the back projection or modified Newton-Raphson algorithm. Therefore, there is no need to store the past measurements in order to estimate the present state.

3.2.3. Inverse solver with IMM algorithm. The IMM algorithm originally proposed by Blom *et al.* [2], has been known as the most cost effective algorithm (performance versus complexity) among the multiple model (MM) algorithms. One of the first applications of the IMM is the work of [2] for air traffic control (ATC). The IMM estimation algorithm has triggered a large variety of related approaches to target tracking [13] and fault detection and diagnosis [20], to name just a few.

The particular behaviour of the IMM algorithm demonstrated in this application also sets it apart from other applications. Whereas the general idea underlying the IMM algorithm is to combine multiple models in order to decide which model gives the best fit with the measurements, what is specific to this application is that these models only differ in their rate of evolution (here, different process covariance matrices).

The IMM algorithm is composed of an estimate mixer at the input of each model-conditioned filter, a bank of the EKFs running simultaneously, a model probability evaluator, and an estimate combiner at the output of the filters. The flow diagram of the IMM algorithm for 1 cycle is depicted in Figure 1. The multiple models interact through the mixing to estimate the time-varying boundary representation. With the assumption that the model transition is governed by an underlying Markov chain, the mixed estimate to each filter is obtained based on the model probabilities and the model transition probabilities. In the filtering stage, each EKF uses a mixed estimate and a voltage measurement to compute a new estimate. The model probabilities are evaluated based on the model transition probabilities, the model likelihoods obtained from the filter residuals and corresponding covariances, and the prior model probabilities. Finally the overall state estimate is computed in the form of the weighted sum of the new estimates and their model probabilities.

The IMM algorithm for M models to estimate the time-varying boundary representation is summarized in the following 4 steps. More detailed derivation and explanation of the IMM are given in [1, 13].

(i) Step 1: Mixing (interaction) of the estimates

Starting with measurement-updated states and covariances from the previous cycle, the mixed initial condition for the j-th filter can be computed as:

- mixing estimate

$$\gamma_{k|k}^{0j} = \sum_{i=1}^{M} \gamma_{k|k}^{i} \, \mu_k^{i|j} \tag{29}$$

- mixing covariance

$$C_{k|k}^{0j} = \sum_{i=1}^{M} [C_{k|k}^{i} + (\gamma_{k|k}^{0j} - \gamma_{k|k}^{i})(\gamma_{k|k}^{0j} - \gamma_{k|k}^{i})^T] \, \mu_k^{i|j} \tag{30}$$

where $\gamma_{k|k}^{0j}$ and $C_{k|k}^{0j}$ represent mixed state and error covariance, respectively, for the input of the j-th model-conditioned EKF. $\mu_k^{i|j}$ in (29) and (30) is the mixing probability (the weight with which the estimates from the previous cycle are given to each filter at the beginning of the current cycle), defined by

$$\mu_k^{i|j} \equiv \frac{1}{\bar{c_j}} \, \pi_{ij} \, \mu_k^{i} \tag{31}$$

where the normalizing constant $\bar{c_j}$ is calculated by

$$\bar{c_j} = \sum_{i=1}^{M} \pi_{ij} \, \mu_k^{i} \tag{32}$$

where π_{ij} is the assumed Markovian transition probability from model i to model j, which is defined by

$$\pi_{ij} \equiv Pr\{M_{k+1}^{j} | M_k^{i}\}, \;\; \forall M^i, M^j \in M^s \tag{33}$$

where $Pr\{\cdot\}$ is probability and M_k^i is the event that i-th mode is in effect at sampling time k, and M^s is the set of all possible modal states at all times.

(ii) Step 2: Model-conditioned filtering

Based on Subsection 3.2.2 two stages of the model-conditioned EKF can be summarized as

- time update (prediction)

$$\gamma_{k+1|k}^{j} = F_k \, \gamma_{k|k}^{0j} \tag{34}$$

$$C_{k+1|k}^{j} = F_k \, C_{k|k}^{0j} \, (F_k)^T + Q_k^j \tag{35}$$

- measurement update (filtering)

$$G_{k+1}^{j} = C_{k+1|k}^{j} (H_{k+1}^{j})^T (S_{k+1}^{j})^{-1} \tag{36}$$

$$\gamma_{k+1|k+1}^{j} = \gamma_{k+1|k}^{j} + G_{k+1}^{j} \, e_{k+1}^{j} \tag{37}$$

$$C_{k+1|k+1}^{j} = (I_{2SN_\theta}^{j} - G_{k+1}^{j} \, H_{k+1}^{j}) \, C_{k+1|k}^{j} \tag{38}$$

where $G_{k+1}^{j} \in \mathbb{R}^{2SN_\theta \times (L+2SN_\theta)}$ is the Kalman gain at time $(k+1)T$. The residuals and their covariances are defined as:

$$e_{k+1}^{j} \equiv \bar{y}_{k+1}^{j} - H_{k+1}^{j} \, \rho_{k+1|k}^{j} \tag{39}$$

$$S_{k+1}^{j} \equiv H_{k+1}^{j} \, C_{k+1|k}^{j} \, (H_{k+1}^{j})^T + \Gamma_{k+1} \tag{40}$$

where pseudo-measurement $\bar{y}_{k+1}^{j}$ and covariance matrix Γ_{k+1} are given by (20) and (23) in Subsection 3.2.2, respectively.

(iii) Step 3: Model probability evaluation

- likelihood function

$$L_{k+1}^{j} = \frac{1}{\sqrt{2\pi|S_{k+1}^{j}|}} \exp[-\tfrac{1}{2}(e_{k+1}^{j})^{T}(S_{k+1}^{j})^{-1}e_{k+1}^{j}] \tag{41}$$

- model probability update

$$\mu_{k+1}^{j} = \frac{1}{c} L_{k+1}^{j}\, \bar{c_j} \tag{42}$$

where

$$c = \sum_{i=1}^{M} L_{k+1}^{i}\, \bar{c_i}. \tag{43}$$

The model probability (42) is updated according to the probability measure (likelihood function (41)), which is calculated based on the residual (39) and its covariance (40) of the corresponding EKF. Note that the residual error defined in (39) is calculated as the difference between measured and calculated voltage. It should be pointed out that the model probability is increased in cases where the residual is decreased.

(iv) Step 4: Combination of estimates

- overall state estimates

$$\gamma_{k+1|k+1} = \sum_{j=1}^{M} \gamma_{k+1|k+1}^{j}\, \mu_{k+1}^{j} \tag{44}$$

- overall error covariance estimates

$$C_{k+1|k+1} = \sum_{j=1}^{M} [C_{k+1|k+1}^{j} + (\gamma_{k+1|k+1} - \gamma_{k+1|k+1}^{j})(\gamma_{k+1|k+1} - \gamma_{k+1|k+1}^{j})^{T}]\, \mu_{k+1}^{j}. \tag{45}$$

Therefore the overall state estimates are computed in the form of the weighted sum of each state estimate. It should be noted that this combination step is only for output purposes and it is not part of the recursive algorithm. In the computational procedure of the IMM algorithm depicted in Figure 1 and summarized in (29)-(45), the following initial guesses need to be chosen before the computations: $\gamma_{0|0}^{i}$, $C_{0|0}^{i}$, μ_{0}^{i}, π_{ij}, Q^{i} $(i, j = 1, 2, \ldots, M)$, and $\bar{R}$.

4. NUMERICAL RESULTS

In order to illustrate the estimation performance of the proposed algorithm we carried out the computer simulations using synthetic data by the FEM. We have considered changing boundary scenarios in the body and trigonometric currents, injected into the circular domain with 15 cm in diameter through 32 electrodes. For the current injection we used the trigonometric current patterns which can be defined as

$$I_{k}^{l} = \begin{cases} \cos(k\theta_l), & l = 1, \ldots, L,\ k = 1, \ldots, L/2 \\ \sin((k - L/2)\theta_l), & l = 1, \ldots, L,\ k = L/2 + 1, \ldots, L - 1 \end{cases} \tag{46}$$

where $\theta_l = 2\pi l/L$. In the forward computations we used the FEM with a mesh of 2736 triangular elements (N_e) and 1497 nodes (N_n). For the simulated boundary and, for the simplicity of the analysis, we set the number of the objects S to be one and the number of basis functions N_θ to be 3 in (4). In the inverse computations we used the FEM with a mesh of 684 triangular elements (N_e) and 407 nodes (N_n) to reduce the computational burden. The electrode contact impedances (z) were assumed to be known constants.

We assume that the object and background resistivities are known and the values are 250×10^6 and 250, respectively. The parameters used for the simulations were as follows: The regularization parameter α was set to 0.01. In the design of the three EKFs, the covariance matrices were assumed to be time invariant and diagonal; the covariance matrices for the measurement noise $\bar{R}_k$ was set to $3 \times 10^2 I_L$, and covariance matrices for the process noise were $Q_k^1 = 0.1 \times I_{2SN_\theta}$, $Q_k^2 = 0.5 \times I_{2SN_\theta}$, and $Q_k^3 = 1 \times I_{2SN_\theta}$. For the initial state vector ($\gamma_{0|0}^{i}$, $i = 1, 2, 3$) of the EKFs we used the circle boundary which has the center $(5, 0)$ and diameter 5 cm, while the initial values of the error covariance matrices ($C_{0|0}^{i}$, $i = 1, 2, 3$) were set to be the identity matrices. In the design of the IMM, the Markov chain transition probabilities π_{ij} are assumed to be 0.8 for $i = j$ and 0.1 for $i \neq j$. In general, the final results were not very sensitive to these parameters (e.g., π_{ii} can be between 0.8 and 0.99). As can be expected, the lower (higher) value will yield less (more) error during transient intervals but more (less) error during quiescent periods. The initial model probabilies (μ_{0}^{i}, $i = 1, 2, 3$) are set to $\frac{1}{3}$.

4.1. The first simulation

For the generation of the changing boundaries, it is assumed that a elliptic target was moved abruptly in a counter clockwise direction after every eight current patterns. The boundaries of the true targets for 1 classical frame are shown with bold line in Figure 2. The first, second, and third columns of Figure 2 are reconstructed boundaries from each EKF with different process covariances and shown with thin line. It should be pointed out that estimation performance of the single EKF heavily depends on the magnitude of the process noise covariance in the random walk model due to its modeling uncertainty. The fourth column shows the reconstructed boundaries obtained by the IMM approach. As it can be seen, the IMM yields better estimates than the EKFs.

The model probability (μ_k^i, $i = 1, 2, 3$) of each single EKF employed in the IMM is depicted in Figure 3. As it can be seen from Figure 3, the model probabilities of the IMM scheme switch rapidly since each EKF has its own dominant intervals and the IMM decides which model gives the best fit with the measurements. In this case the EKF1 and EKF2 is dominant alternately, while the EKF3 is insignificant

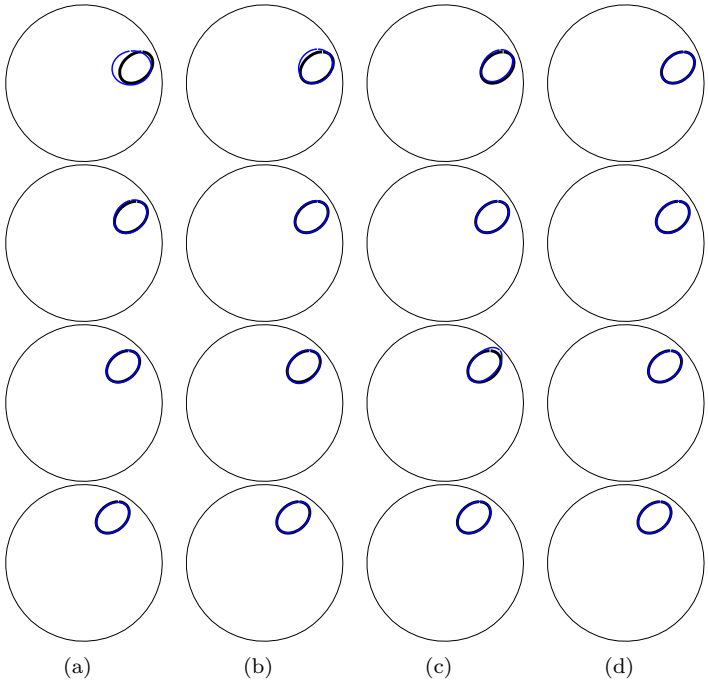

Figure 2. The reconstructed boundaries in the first simulation. The true boundaries are bold lines and the reconstructed boundaries are thin lines: (a) boundaries reconstructed by the EKF1, (b) boundaries reconstructed by the EKF2, (c) boundaries reconstructed by the EKF3, and (d) boundaries reconstructed by the IMM.

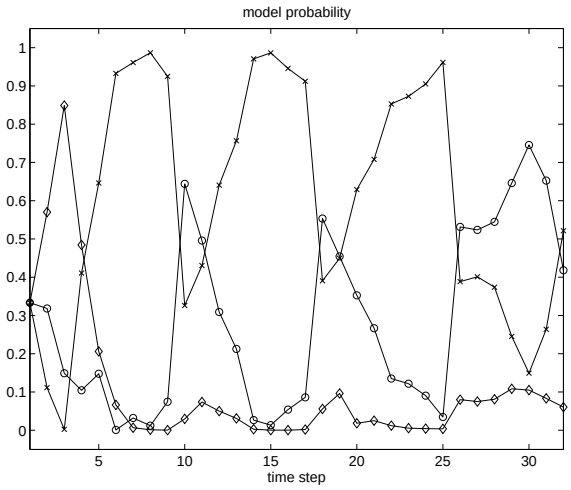

Figure 3. Model probabilities for each model (EKF1: –X–, EKF2: –O–, EKF3: –◇–).

for almost all intervals.

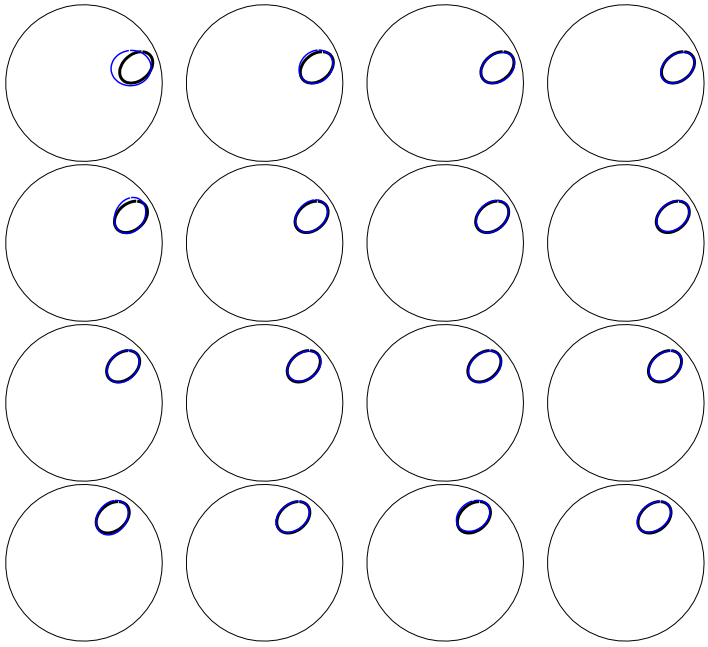

Figure 4. The reconstructed boundaries in the second simulation. The true boundaries are bold lines and the reconstructed boundaries are thin lines: (a) boundaries reconstructed by the EKF1, (b) boundaries reconstructed by the EKF2, (c) boundaries reconstructed by the EKF3, and (d) boundaries reconstructed by the IMM.

4.2. The second simulation

In the second simulation, we added zero-mean Gaussian noise to the calculated voltages to generate noisy measurements; the noise level was set to be 1% of the corresponding calculated voltages. The other parameters used in the reconstruction were the same as in the first simulation. The boundaries of the true targets for 1 classical frame are shown with bold line in Figure 4. The first, second, and third columns of Figure 4 are reconstructed boundaries from each EKF with different process covariances and shown with thin line. The visual quality of the reconstructed boundaries from the IMM approach is enhanced compared to that of the boundaries from each of the EKFs.

5. CONCLUSIONS

We addressed a special class of the EIT inverse problem, in which position and shape of the objects were the unknowns to be identified in stead of resistivity itself. In particular, it was assumed that these unknowns are nonstationary within the time taken to acquire a full set of measurement data. The boundary of the object was formulated as truncated Fourier series and time-varying Fourier coefficients were estimated with the aid of the IMM algorithm, following the voltage measurements corresponding to each current pattern. In doing so, multiple models with different process noise covariances are employed to alleviate the modeling uncertainty of the random walk model. A spatial regularization scheme was employed to mitigate the ill-posedness of the problem.

The proposed boundary estimation scheme based on the IMM is a on-line recursive estimator, in which there is no need to store the past measurements in order to estimate the present state. The IMM approach employed in this paper consists of a bank of model-conditioned extended Kalman filters connected in parallel, a model probability evaluator, an estimate mixer at the input of each Kalman filter, and an estimate combiner at the output of the parallel filters.

Acknowledgments

This work was supported by grant No. R01-2002-000-0040-0 (2004) from the Basic Research Program of the Korea Science and Engineering Foundation.

REFERENCES

1. Y. Bar-Shalom and X.R. Li, *Estimation and Tracking : Principles, Techniques and Software*, Artech House, London, 1993.
2. H.A.P. Blom and Y. Bar-Shalom, The interacting multiple model algorithm for systems with Markovian switching coefficients. *IEEE Trans. Automat. Contr.* (1998), **33**, 780-783.
3. M. Cheney, D. Isaacson, J.C. Newell, S. Smike and J. Goble, NOSER: An algorithm for solving the inverse conductivity problem. *Int. J. Imaging Syst. Technol.* (1990), **2**, 65-75.
4. A. Gelb, *Applied Optimal Estimation*, M.I.T. Press, Massachusetts, 1974.
5. D.K. Han and A. Prosperetti, A shape decomposition technique in electrical impedance tomography. *J. Comput. Phys.* (1999), **155**, 75-95.
6. P. Hua, E.J. Woo, J.G. Webster and W.J. Tompkins, Iterative reconstruction methods using regularization and optimal current patterns in electrical impedance tomography. *IEEE Trans. Med. Imaging* (1991), **10**, 621-628.
7. B.S. Kim, M.C. Kim, S. Kim and K.Y. Kim, Nonstationary electrical impedance Tomography with the IMM scheme. *Meas. Sci. Technol.* (2004), **15**, 2113-2123.
8. K.Y. Kim, B.S. Kim, M.C. Kim, S. Kim, D. Isaacson and J.C. Newell, Dynamic electrical impedance imaging with the interacting multiple model scheme. *Physiol. Meas.* (2004), (*Accepted for publication*).
9. K.Y. Kim, B.S. Kim, M.C. Kim, Y.J. Lee and M. Vauhkonen, Image reconstruction in time-varying electrical impedance tomography based on the extended Kalman filter. *Meas. Sci. Technol.* (2001), **12**, 1032-1039.
10. M.C. Kim, S. Kim and K.Y. Kim, Estimation of phase boundaries in two-phase systems by electrical impedance tomography technique. *J. Indus. Eng. Chem.* (2004), **10**, 710-716.
11. V. Kolehmainen, S.R. Arridge, W.R.B. Lionheart, M. Vauhkonen and J.P. Kaipio, Recovery of region boundaries of piecewise constant coefficients of an elliptic PDE from boundary data. *Inverse Problems* (1999), **15**, 1375-1391.
12. V. Kolehmainen, A. Voutilainen, and J.P. Kaipio, Estimation of non-stationary region boundaries in EIT - state estimation approach. *Inverse Problems* (2001), **17**, 1937-1956.
13. E. Mazor, A. Averbuch, Y. Bar-Shalom and J. Dayan, Interacting multiple model methods in target tracking: A survey. *IEEE Trans. Aero. Elec. Sys.* (1998), **34**, 103-123.
14. A. Seppanen, M. Vauhkonen, E. Somersalo and J.P. Kaipio, State space models in process tomography-approximation of state noise covariance. *Inverse Problems Eng.* (2001), **9**, 561-585.
15. E. Somersalo, M. Cheney and D. Isaacson, Existence and uniqueness for electrode models for electric current computed tomography. *SIAM J. Appl. Math.* (1992), **52**, 1023-1040.
16. M. Vauhkonen, Electrical impedance tomography and prior information. *PhD Thesis*, University of Kuopio, Finland, 1997.
17. M. Vauhkonen, P.A. Karjalainen and J.P. Kaipio, A Kalman filter approach applied to the tracking of fast movements of organ boundaries in electrical impedance tomography. *Proc. 20th Ann. Int. Conf. IEEE Eng. Med. Biol. Soc.*, Hong Kong Sar, China, 1998, pp.1048-1051.
18. J.G. Webster, *Electrical Impedance Tomography*, Adam Hilger, Bristol, 1990.
19. T.J. Yorkey, J.G. Webster and W.J. Tompkins, Comparing reconstruction algorithms for electrical impedance tomography. *IEEE Trans. Biomed. Eng.* (1987), **34**, 843-852.
20. Y. Zhang and X.R. Li, Detection and diagnosis of sensor and actuator failures using IMM estimator. *IEEE Trans. Aero. Elec. Sys.* (1998), **34**, 1293-1313.